PERGAMON

International Journal of Plasticity 15 (1999) 1359–1378

INTERNATIONAL JOURNAL OF Plasticity

A return-map algorithm for general associative isotropic elasto-plastic materials in large deformation regimes

F. Auricchio [a,*], R.L. Taylor [b]

[a] *Dipartimento di Meccanica Strutturale, Università di Pavia, Via Ferrata 1, 27100 Pavia, Italy*
[b] *Department of Civil Engineering, University of California at Berkeley, Davis Hall, Berkeley, CA 94720, USA*

Received in final revised form 20 September 1999

Abstract

The present paper addresses a flexible solution algorithm for associative isotropic elasto-plastic materials, i.e. for materials whose elastic and plastic behaviors are described through an isotropic free-energy function, an isotropic yield function and an associative flow rule. The discussion is relative to a large deformation regime, while no hardening mechanisms are included. The algorithm is based on a combination of the operator split method and a return map scheme. Both the algorithm linearization and the requirements for the yield criterion convexity are discussed in detail. Finally, to show the algorithm flexibility and performance, the discussion is specialized to three yield criteria and some test problems are studied. © 1999 Elsevier Science Ltd. All rights reserved.

Keywords: B. Elastic–plastic; Finite strain; C. Finite elements; Numerical algorithms; Return map

1. Introduction

The goal of the present paper is to devise and discuss a flexible solution algorithm for general associative isotropic elasto-plastic materials, i.e. for materials whose elastic and plastic behaviors are described respectively through an isotropic free-energy function,[1] an isotropic yield function and an associative flow rule. The discussion is

* Corresponding author.
E-mail address: auricchio@unipv.it (F. Auricchio).

[1] Indicating with **x** a second order tensor, g is an isotropic function of **x** if it depends on **x** only through its invariants.

0749-6419/99/$ - see front matter © 1999 Elsevier Science Ltd. All rights reserved.
PII: S0749-6419(99)00044-3

relative to a large deformation regime and only isotropic hardening mechanisms are included in the modelling.

The motivation of the work is mainly related to the more and more frequent use of new materials in the engineering practice, such as laminated composites, shape-memory alloys and many others. In fact, experimental investigations often show the need to introduce quite general and complex yield criteria to describe the inelastic behavior of these materials. Accordingly, we found it useful to devise an algorithm not strictly related to a specific yield locus. In fact, the main advantage of the proposed approach is the possibility to easily introduce different yield criteria and, hence, to easily experiment with them in a general large deformation finite-element context.

The paper is organized as follows. Section 2 reviews the constitutive equations governing the behavior of general associative isotropic elasto-plastic materials and the requirements for convexity of yield criteria. Section 3 addresses a possible solution strategy within a time-discrete framework, while Section 4 specializes the previous considerations to a particular form of free-energy and to three different yield criteria. Finally, Section 5 presents some numerical simulations to show the performance of the algorithm for the constitutive models considered.

2. Time-continuous constitutive equations

We consider a continuum undergoing large deformations. In particular, relying on continuum mechanics theory as presented in classical textbooks (Gurtin, 1981), in the following we avoid as much as possible the repetition of well-established concepts.

We introduce a local multiplicative decomposition of the deformation gradient $\mathbf{F}$ in the form:

$$\mathbf{F} = \mathbf{F}^e \mathbf{F}^p \tag{1}$$

where $\mathbf{F}^e$ represents the elastic part of the deformation gradient and $\mathbf{F}^p$ is an internal variable related to the evolution of inelastic processes (Lee, 1969; Mandel, 1974). Accordingly, the elastic right Cauchy–Green tensor $\mathbf{C}^e$ and the elastic left Cauchy–Green tensor $\mathbf{b}^e$ can be defined respectively as:

$$\mathbf{C}^e = \mathbf{F}^{e,T} \mathbf{F}^e \tag{2}$$

$$\mathbf{b}^e = \mathbf{F}^e \mathbf{F}^{e,T}$$

where the superscript T indicates the transpose. In the forthcoming discussion we assume $\mathbf{b}^e$ as the internal variable (Simo and Hughes, 1998), recalling the relation:

$$\mathbf{b}^e = \mathbf{F}[\mathbf{C}^p]^{-1} \mathbf{F}^T \tag{3}$$

with:

$$\mathbf{C}^p = \mathbf{F}^{p,T} \mathbf{F}^p \tag{4}$$

2.1. Free-energy and elastic relation

Consistent with the assumption of an isotropic elastic response, the free-energy is assumed to be an isotropic function of the elastic left Cauchy–Green tensor $\mathbf{b}^e$; hence:

$$\psi = \psi(\mathbf{b}^e) \tag{5}$$

Accordingly, the Kirchhoff stress $\boldsymbol{\tau}$ is given by:

$$\boldsymbol{\tau} = 2\frac{\partial \psi}{\partial \mathbf{b}^e}\mathbf{b}^e \tag{6}$$

Due to isotropy, the principal directions of the Kirchhoff stress $\boldsymbol{\tau}$ and of the elastic left Cauchy–Green tensor $\mathbf{b}^e$ coincide. Hence, indicating such principal directions with $\mathbf{n}^{\mathrm{A}}$,[2] the following spectral decompositions can be introduced:

$$\boldsymbol{\tau} = \sum_{\mathrm{A}=1}^{3} \tau_{\mathrm{A}} \mathbf{n}^{\mathrm{A}} \otimes \mathbf{n}^{\mathrm{A}} \tag{7}$$

$$\mathbf{b}^e = \sum_{\mathrm{A}=1}^{3} (\lambda_{\mathrm{A}}^e)^2 \mathbf{n}^{\mathrm{A}} \otimes \mathbf{n}^{\mathrm{A}}$$

Eq. 6 can then be rewritten in scalar form as:

$$\begin{aligned} &\tau_A = 2\frac{\partial \psi}{\partial\left[(\lambda_A^e)^2\right]}(\lambda_A^e) \\ &\text{or as :} \\ &\tau_{\mathrm{A}} = \frac{\partial \psi}{\partial \psi_{\mathrm{A}}^e} \end{aligned} \tag{8}$$

as shown in the Appendix. Moreover, the Kirchhoff stress $\boldsymbol{\tau}$ can be split into its volumetric and deviatoric part as follows:

$$\boldsymbol{\tau} = p\mathbf{1} + \mathbf{t} \tag{10}$$

where $\mathbf{1}$ is the second order identity tensor, $p = (\boldsymbol{\tau} : \mathbf{1})/3$ with the ":" indicating a double contraction between second order tensors, and $\mathbf{t} = \boldsymbol{\tau} - p\mathbf{1}$, the latter having the following spectral representation:

$$\mathbf{t} = \sum_{\mathrm{A}=1}^{3} t_{\mathrm{A}} \mathbf{n}^{\mathrm{A}} \otimes \mathbf{n}^{\mathrm{A}} \tag{11}$$

with:

$$t_{\mathrm{A}} = \tau_{\mathrm{A}} - p \tag{12}$$

[2] Note that: (1) the index range is {1,2,3} and it is in general omitted in the forthcoming equations; (2) summations are always explicitly indicated, i.e. no summation convention is assumed to be valid.

2.2. Yield criterion and plastic evolution

Consistent with the assumption of isotropic plastic response, the yield function F is chosen to be an isotropic function of the Kirchhoff stress. Excluding hardening mechanisms from the modelling:

$$F(I_1, J_2, J_3) = f(I_1, J_2, J_3) - \sigma_Y \tag{13}$$

where I_1, J_2, J_3 are the three stress invariants, defined as:

$$I_1 = \boldsymbol{\tau} : \mathbf{1} = \tau_1 + \tau_2 + \tau_3 \tag{14}$$

$$J_2 = \frac{1}{2}\mathbf{t}^2 : \mathbf{1} = \frac{1}{2}(t_1^2 + t_2^2 + t_3^2)$$

$$J_3 = \frac{1}{3}\mathbf{t}^3 : \mathbf{1} = \frac{1}{3}(t_1^3 + t_2^3 + t_3^3)$$

and σ_Y is a scalar material constant, representing the radius of the yield function (Lubliner, 1990). Following Simo (1992, 1999), Simo and Meschke (1993) and Simo and Hughes (1998), the model is completed by introducing the associative evolution equation for $\mathbf{b}^e$:

$$-\frac{1}{2}\mathcal{L}\boldsymbol{\nu}\mathbf{b}^e = \dot{\gamma}\mathbf{N}\mathbf{b}^e \tag{15}$$

and the Kuhn–Tucker conditions:

$$\dot{\gamma} \geqslant 0, F \leqslant 0, \dot{\gamma}F = 0 \tag{16}$$

where:

- $\mathcal{L}_{\boldsymbol{\nu}}\mathrm{b}^e$ is the Lie derivative of $\mathbf{b}^e$ defined as:

$$\mathcal{L}_{\boldsymbol{\nu}}\mathrm{b}^e = \mathbf{F}^T \frac{\partial}{\partial t}\left[(\mathbf{C}^p)^{-1}\right]\mathbf{F} \tag{17}$$

with t indicating a pseudo-time variable

- $\dot{\gamma}$ is the plastic consistency parameter
- $\mathbf{N}$ is the normal to the yield function, defined as:

$$\mathbf{N} = \frac{\partial F}{\partial \boldsymbol{\tau}} \tag{18}$$

We observe that $\mathbf{N}$ has the same spectral representation as $\boldsymbol{\tau}$ and $\mathbf{t}$, i.e.:

$$\mathbf{N} = \sum_{\mathrm{A}=1}^{3} N_{\mathrm{A}}\mathbf{n}^{\mathrm{A}} \otimes \mathbf{n}^{\mathrm{A}} \tag{19}$$

In fact, noting that:

$$\frac{\partial \mathbf{t}}{\partial \boldsymbol{\tau}} = \mathbf{I} - \frac{1}{3}\mathbf{1} \otimes \mathbf{1} \tag{20}$$

where $\mathbf{I}$ is the fourth-order identity tensor, we have:

$$\frac{\partial I_1}{\partial \boldsymbol{\tau}} = \mathbf{1}, \frac{\partial J_2}{\partial \boldsymbol{\tau}} = \mathbf{t}, \frac{\partial J_3}{\partial \boldsymbol{\tau}} = \mathbf{t}^2 - \frac{2}{3}J_2\mathbf{1} \tag{21}$$

and:

$$\mathbf{N} = \frac{\partial F}{\partial \boldsymbol{\tau}} = F_1\mathbf{1} + F_2\mathbf{t} + F_3(\mathbf{t}^2 - \frac{2}{3}J_2\mathbf{1}) = (F_1 - \frac{2}{3}F_3J_2)\mathbf{1} + F_2\mathbf{t} + F_3\mathbf{t}^2 \tag{22}$$

with:

$$F_1 = \frac{\partial F}{\partial I_1}, F_2 = \frac{\partial F}{\partial J_2}, F_3 = \frac{\partial F}{\partial J_3} \tag{23}$$

2.3. Convexity of the yield criterion: some considerations

As an aside remark, it is interesting to note that the derivations presented so far allow some considerations on the yield function convexity[3] (Lubliner, 1990). In fact, to verify the convexity of F, it is sufficient to guarantee that the matrix:

$$\mathbf{H} = \left[\frac{\partial^2 F}{\partial \boldsymbol{\tau}\partial \boldsymbol{\tau}}\right] \tag{24}$$

is positive semi-definite (Protter et al., 1992). From the previous results, it is possible to give a closed form of the matrix $\mathbf{H}$.

In fact, from Eq. (22), we have:

$$\begin{aligned}\frac{\partial^2 F}{\partial \boldsymbol{\tau}\partial \boldsymbol{\tau}} &= \frac{\partial \mathbf{N}}{\partial \boldsymbol{\tau}} \\ &= \mathbf{1} \otimes \left[F_{11}\frac{\partial I_1}{\partial \boldsymbol{\tau}} + F_{12}\frac{\partial J_2}{\partial \boldsymbol{\tau}} + F_{13}\frac{\partial J_3}{\partial \boldsymbol{\tau}}\right] \\ &+ \mathbf{t} \otimes \left[F_{21}\frac{\partial I_1}{\partial \boldsymbol{\tau}} + F_{22}\frac{\partial J_2}{\partial \boldsymbol{\tau}} + F_{23}\frac{\partial J_3}{\partial \boldsymbol{\tau}}\right] + F_2\frac{\partial \mathbf{t}}{\partial \boldsymbol{\tau}} \\ &+ \left[\mathbf{t}^2 - \frac{2}{3}J_2\mathbf{1}\right] \otimes \left[F_{31}\frac{\partial I_1}{\partial \boldsymbol{\tau}} + F_{32}\frac{\partial J_2}{\partial \boldsymbol{\tau}} + F_{33}\frac{\partial J_3}{\partial \boldsymbol{\tau}}\right] \\ &+ F_3\left[\frac{\partial(\mathbf{t}^2)}{\partial \boldsymbol{\tau}} - \frac{2}{3}\mathbf{1} \otimes \frac{\partial J_2}{\partial \boldsymbol{\tau}}\right]\end{aligned} \tag{25}$$

[3] We wish to stress that the yield function convexity is by no means a necessary condition on the derivations presented so far or on the forthcoming numerical solution algorithm.

where the double pedices indicate a double derivative operation, consistent with the notation introduced in Eq. (23). Since $F_{AB} = F_{BA}$ and recalling Eq. (21), we finally obtain the form:

$$\begin{aligned}\frac{\partial^2 F}{\partial\boldsymbol{\tau}\partial\boldsymbol{\tau}} &= F_2\mathbf{I} + 2F_3\mathbf{T} + (F_{11} - \frac{1}{3}F_2)[\mathbf{1}\otimes\mathbf{1}] + F_{22}[\mathbf{t}\otimes\mathbf{t}] \\ &\quad + (F_{12} - \frac{2}{3}F_3)[\mathbf{1}\otimes\mathbf{t} + \mathbf{t}\otimes\mathbf{1}] + F_{33}[\mathbf{d}\otimes\mathbf{d}] + [\mathbf{a}\otimes\mathbf{d} + \mathbf{d}\otimes\mathbf{a}]\end{aligned} \tag{26}$$

with:

$$\mathbf{T} = \frac{\partial}{\mathbf{t}}[\mathbf{t}^2] \tag{27}$$

$$\mathbf{a} = F_{23}\mathbf{t} + F_{13}\mathbf{1}$$

$$\mathbf{d} = \mathbf{t}^2 - \frac{2}{3}J_2\mathbf{1}$$

Global convexity of the yield function is guaranteed if all the principal minors of $\partial^2 F/\partial\boldsymbol{\tau}\partial\boldsymbol{\tau}$ are non-negative (Protter et al., 1992).

3. Time-discrete constitutive equations and solution algorithm

We now solve the non-linear problem described in Section 2 in a discrete set of time increments (time-discrete problem). Prom a computational standpoint we treat the non-linear material behavior as *configuration-driven*, adopting in particular an updated-Lagrangian approach (Bathe, 1982). Accordingly, let $[0, T] \subset \mathrm{IR}$ be the time interval of interest and t_n a time instant in which the solution is known (i.e. indicating with a subscript n a quantity evaluated at time t_n, we assume to know $\mathbf{F}_n$ and $\mathbf{b}_n^e$). Then, indicating with t a time instant after t_n and assuming to know also the current configuration (i.e. $\mathbf{F}$), we wish to solve the non-linear evolutionary problem over the time interval $[t_n, t]$. To reach this goal and following Simo (1992), we introduce the relative deformation gradient $\mathbf{f}$, satisfying the relation:

$$\mathbf{F} = \mathbf{f}\mathbf{F}_n \tag{28}$$

and we go through the following steps:

1. split the time-continuous problem into two simpler sub-problems,
2. introduce a time-discrete counterpart of the two sub-problems, and
3. address the solution algorithm for the two time-discrete sub-problems.

3.1. Time-continuous operator split

The non-linear problem under investigation is initially tackled via the operator split method. Accordingly, the following two time-continuous subproblems are introduced:

- *Time-continuous sub-problem 1 [TC-P1]*. This problem is obtained from the original one by freezing the plastic flow in the time interval $[t_n, t]$. Accordingly, the sub-problem consists in:
  - computing a relative deformation gradient solving Eq. (28)
  - computing an update elastic left Cauchy–Green tensor assuming that all the relative deformation gradient $\mathbf{f}$ is elastic; clearly, this updated elastic left Cauchy–Green tensor would not necessarily be the solution of the complete elasto-plastic problem. Accordingly, adopting a superscript TR to indicate trial quantities, we have:

$$\mathbf{b}^{e,TR} = \mathbf{f}\mathbf{b}_n^e\mathbf{f}^T \tag{29}$$

- *Time-continuous sub-problem 2 [TC-P2]*. The second problem is obtained from the original one considering the configuration fixed (i.e. $\mathbf{F}$ is given and set) and solving on such known configuration the plastic evolutionary problem, starting from the trial solution of sub-problem 1. Accordingly, the equations governing sub-problem 2 are:

$$\dot{\mathbf{b}}^e = -2\dot{\gamma}\mathbf{N}\mathbf{b}^{e,TR} \tag{30}$$

$$\dot{\gamma} \geqslant 0,\ F \leqslant 0,\ \dot{\gamma}F = 0 \tag{31}$$

3.2. Time-discrete sub-problems

We now consider a given time instant $t_{n+1} > t_n$, with t_{n+1} being the first discrete time value of interest after t_n; the goal is to construct a time-discrete algorithmic counterpart of the two sub-problems over the time interval $[t_n, t_{n+1}]$.

The time-discrete counterpart of TC-P1 (indicated as TD-PI and representing the computation of the trial state) is trivial, being just a configuration update and a push-forward of the elastic left Cauchy–Green strain tensor to compute $\mathbf{b}^{e,TR}$, as indicated in Eq. (29).

The time-discrete counterpart of TC-P2 (indicated as TD-P2 and representing the computation of the plastic evolution) is on the other hand more complicated, mainly for the presence of the Kuhn–Micker constraint equations.

$$\Delta\gamma = \int_{t_n}^{t_{n+1}} \dot{\gamma}\,\mathrm{d}t \tag{32}$$

and using an exponential approximation for the rate equation (30), the time-discrete evolution of $\mathbf{b}^e$ is governed by the following equation:

$$\mathbf{b}^e = \exp[-2\Delta\gamma\mathbf{N}]\mathbf{b}^{e,TR} \tag{33}$$

where the subscript $n+1$ is omitted to indicate quantities evaluated at time t_{n+1}. Recalling that $\mathbf{b}^e$ and $\mathbf{N}$ have the same spectral decomposition, Eq. (33) implies that also $\mathbf{b}^e$ and $\mathbf{b}^{e,TR}$ have the same spectral decomposition (i.e. $\mathbf{n}_{\mathrm{A}}^{TR} = \mathbf{n}_{\mathrm{A}}$); accordingly, Eq. (33) can be transformed into three scalar equations relative to the space of principal directions:

$$\lambda_{\mathrm{A}}^{e} = \exp[-\Delta\gamma N_A]\lambda_{\mathrm{A}}^{e,TR} \tag{34}$$

where $\lambda_{\mathrm{A}}^{e,TR}$ and N_{A} are, respectively the eigenvalues of $\mathbf{b}^{e,TR}$ and $\mathbf{N}$. Taking the logarithm of both sides of Eq. (34), we get:

$$\log\left[\lambda_{\mathrm{A}}^{e}\right] = -\Delta\gamma N_{\mathrm{A}} + \log\left[\lambda_{\mathrm{A}}^{e,TR}\right] \tag{35}$$

Finally, introducing now the principal elastic logarithmic strains:

$$\varepsilon_{\mathrm{A}}^{e} = \log\left[\lambda_{\mathrm{A}}^{e}\right],\ \varepsilon_{\mathrm{A}}^{e,TR} = \log\left[\lambda_{\mathrm{A}}^{e,TR}\right] \tag{36}$$

the time-discrete sub-problem 2 can be reformulated as:

$$\varepsilon_{\mathrm{A}}^{e} = \varepsilon_{\mathrm{A}}^{e,TR} - \Delta\gamma N_{\mathrm{A}} \tag{37}$$

$$\Delta\gamma \geqslant 0,\ F \leqslant 0,\ \Delta_{\gamma} F = 0 \tag{38}$$

3.3. Return map algorithm

We may now observe that Eq. (37) closely resembles in form the equations governing a classical time-discrete small deformation plastic evolutionary problem, tackled through a return map method (Simo and Taylor, 1985; Auricchio and Taylor, 1995; Simo and Hughes, 1998). In particular, Eq. (37) can be interpreted as a return map in strain space subjected to the usual Kuhn–Tucker conditions. Accordingly, the elastic strain is equal to the trial elastic strain minus a plastic incremental correction and the non-linear time-discrete sub-problem TD-P2 can be solved as commonly done in the small-deformation regime, i.e.:

- *TD-P2 a*. Check if the trial Kirchhoff stress $\tau_{\mathrm{A}}^{TR}(\lambda_{\mathrm{A}}^{e,TR})$ violates the yield criterion.
- *TD-P2 b*. If the constraint is not violated (i.e. $F(\tau_{\mathrm{A}}^{TR}) \leqslant 0$), the trial state is admissable and it also represents the solution of the TD-P2 problem.
- *TD-P2 c*. If the constraint is violated (i.e. $F(\tau_{\mathrm{A}}^{TR}) > 0$), the trial state is non-admissable and a plastic correction should be performed enforcing the satisfaction of the consistency condition $F = 0$.

Remark 3.1. *The arguments so far presented indicate that the return map can be performed in the space of principal directions. Accordingly, from now on, we assume that the principal directions are known and that all the quantities are expressed with respect to these directions. This implies that all the variables previously considered as second order tensors can now be considered as vectors of three components, i.e. as vectors containing the components relative to the tensor representation in the space of principal directions. As examples,* $\boldsymbol{\varepsilon}^e$, $\boldsymbol{\varepsilon}^{e,TR}$, $\theta\boldsymbol{\tau}$ *and* $\mathbf{N}$ *will now indicate vectors with three components*

$$\boldsymbol{\varepsilon}^e = \left\{\varepsilon_1^e, \varepsilon_2^e, \varepsilon_3^e\right\}^T \text{etc.} \tag{39}$$

and their generic Ath component is given by:

$$\boldsymbol{\varepsilon}^e\big|_A = \varepsilon_A^e,\ \boldsymbol{\varepsilon}^{e,TR}|_A = \varepsilon_A^{e,TR} \tag{40}$$

$$\boldsymbol{\tau}|_A = \tau_A, \mathbf{N}|_A = N_A$$

We now note that the computation of the plastic correction (TD-P2c) requires the solution of a non-linear system. In particular, following the vectorial notation discussed in Remark 3.1 and combining Eq. (13) with the three scalar equations (37) written in residual vectorial form, we obtain:

$$\mathbf{R}_\in = \boldsymbol{\varepsilon}^e(\boldsymbol{\tau}) + \Delta\gamma\mathbf{N} - \boldsymbol{\varepsilon}^{e,TR} = \mathbf{0} \tag{41}$$

$$R_y = F(I_1, J_2, J_3) = 0$$

which is a system of four scalar equations in the four unknowns τ_A and Δ_γ. In fact, $\boldsymbol{\varepsilon}^e$ is a function of τ through the elastic constitutive equations, $\mathbf{N}$ is a function of $\boldsymbol{\tau}$ as shown in Eq. (22), $\boldsymbol{\varepsilon}^{TR}$ is a fixed quantity within the plastic correction step, F is a function of $\boldsymbol{\tau}$ through its invariants and Δ_γ appears explicitly in the first three equations. In a more compact form we have:

$$\mathbf{R} = \mathbf{R}(\mathbf{z}) = \mathbf{0} \tag{42}$$

with $\mathbf{z} = \left\{\boldsymbol{\tau}, \Delta_\gamma\right\}$, the non-linear system can be solved through a classical Newton iterative technique, hence the following linearization is needed:

$$\frac{\partial \mathbf{R}}{\partial z} = \begin{bmatrix} \dfrac{\partial \mathbf{R}_\varepsilon}{\partial \boldsymbol{\tau}} & \dfrac{\partial \mathbf{R}_\varepsilon}{\partial \Delta\gamma} \\ \left(\dfrac{\partial R_y}{\partial \boldsymbol{\tau}}\right)^T & 0 \end{bmatrix} = \begin{bmatrix} \dfrac{\partial \mathbf{R}_\varepsilon}{\partial \boldsymbol{\tau}} & \mathbf{N} \\ \mathbf{N}^T & 0 \end{bmatrix} \tag{43}$$

where:

$$\frac{\partial \mathbf{R}_{\varepsilon}}{\partial \boldsymbol{\tau}} = \frac{\partial \boldsymbol{\varepsilon}^{e}}{\partial \boldsymbol{\tau}} + \Delta\gamma \frac{\partial \mathbf{N}}{\partial \boldsymbol{\tau}} \tag{44}$$

We recall that the expression of $\partial \mathbf{N}/\partial \boldsymbol{\tau}$ has already been derived in Eq. (25) and this is expressed in terms of the second partial derivatives of the yield function F with respect to the stress invariants. The algorithmic details are reported in Table 1.

3.4. Algorithm linearization

We now discuss the linearization of the time-discrete algorithm, leading to the so-called consistent or algorithmic tangent matrix. The use of a consistent tangent preserves the quadratic convergence of a Newton method, which we adopt in the next section for the incremental solution in a finite element scheme.

Following Simo (1992, 1999), Armero and Simo (1993) and Simo and Hughes (1998), the only part of the tangent matrix influenced by the specific constitutive model is the so-called material tangent. In particular, the material tangent can be computed as a linearization of the Kirchhoff stress over a fixed configuration, i.e. as:

$$\frac{\mathrm{d}\boldsymbol{\tau}}{\mathrm{d}\boldsymbol{\varepsilon}} \tag{45}$$

To compute this matrix, we start by considering system (42) as a function of $z = \{\boldsymbol{\tau}, \Delta_{\gamma}\}$ and $\boldsymbol{\varepsilon}$ [i.e. $\mathbf{R} = \mathbf{R}(\mathbf{z}, \boldsymbol{\varepsilon}) = 0$]. Through linearization, we get:

Table 1
Time-discrete solution algorithm

1. Compute trial elastic state a. Compute the elastic trial left Cauchy–Green tensor: $\mathbf{b}^{e,TR} = \mathbf{f}\mathbf{b}_{n}^{e}\mathbf{f}^{T}$ b. Compute the spectral decomposition of $\mathbf{b}^{e,TR}$ Compute $\mathbf{n}^{A,TR} = \mathbf{n}^{A}$ and $\lambda_{\mathrm{A}}^{e,TR}$ c. Compute the trial Kirchhoff stress $\boldsymbol{\tau}^{TR} = \boldsymbol{\tau}^{TR}(\lambda_{\mathrm{A}}^{e,TR})$	(TD-P1)
2. Check yielding condition Check if the trial Kirchhoff stress is admissible or not: $F(\tau_{\mathrm{A}}^{TR}) \begin{cases} < 0 \Rightarrow \text{state is admissible} \\ > 0 \Rightarrow \text{state is non-admissible} \end{cases}$	(TD-P2a)
3. If (trial state admissible) then no solution is required; exit	(TD-P2b)
4. If (trial state non-admissible) then perform plastic correction: $\mathbf{b}^{e} = \exp\left[-2\Delta_{\gamma}\mathbf{N}\right]\mathbf{b}^{e,TR}$ $\Delta\gamma = \int_{t_n}^{t_{n+1}} \dot{\gamma}\,\mathrm{d}t$ with $\Delta\gamma$ and $\boldsymbol{\tau}$ computed solving system (42).	(TD-P2c)

$$\mathrm{d}\mathbf{R} = \frac{\partial \mathbf{R}}{\partial \mathbf{z}}\mathrm{d}\mathbf{z} + \frac{\partial \mathbf{R}}{\partial \boldsymbol{\varepsilon}}\mathrm{d}\boldsymbol{\varepsilon} = \mathbf{0} \tag{46}$$

and solving with respect to $\mathbf{z}$:

$$\mathrm{d}\mathbf{z} = -\left[\frac{\partial \mathbf{R}}{\partial \mathbf{z}}\right]^{-1}\frac{\partial \mathbf{R}}{\partial \boldsymbol{\varepsilon}}\mathrm{d}\boldsymbol{\varepsilon} \tag{47}$$

Noting now that:

$$\frac{\partial \mathbf{R}}{\partial \boldsymbol{\varepsilon}} = \begin{bmatrix} -1 & 0 & 0 \\ 0 & -1 & 0 \\ 0 & 0 & -1 \\ 0 & 0 & 0 \end{bmatrix} \tag{48}$$

we have that:

$$\left.\frac{\partial \boldsymbol{\tau}}{\partial \boldsymbol{\varepsilon}}\right|_{\mathrm{AB}} = \left.\left[\frac{\partial \mathbf{R}}{\partial \mathbf{z}}\right]^{-1}\right|_{\mathrm{AB}} \tag{49}$$

Recalling that the computation of the consistency parameter Δ_γ is performed through a Newton method on system (42), hence requiring an inversion of matrix (43), we may conclude that at the end of the plastic correction step the material tangent is already available!

4. A particular model

All the considerations presented so far are valid for a general associative isotropic elasto-plastic material. To show the flexibility of the proposed framework, we now introduce specific forms for the free-energy ψ and the yield function F, as discussed in the following.

4.1. Free-energy

We assume a free-energy function uncoupled in a deviatoric and a volumetric part:

$$\psi = U(J^e) + W(\bar{\lambda}^e_{\mathrm{A}}) \tag{50}$$

where $J^e = \lambda^e_1\lambda^e_2\lambda^e_3$ is the elastic volume and $\bar{\lambda}^e_{\mathrm{A}} = (J^e)^{-\frac{1}{3}}\lambda^e_{\mathrm{A}}$ are the deviatoric principal stretches. In particular, both U and W are assumed quadratic in the principal elastic logarithmic stretches:

$$U(J^e) = \frac{1}{2}K\{\log[J^e]\}^2 \tag{51}$$

$$W(\bar{\lambda}_A^e) = G\sum_{A=1}^{3}\left\{\log\left[\bar{\lambda}_A^e\right]\right\}^2$$

Noting that:

$$p = \frac{\partial\psi}{\partial J^e}J^e \tag{52}$$

$$t_{\mathrm{A}} = \frac{\partial\psi}{\partial\bar{\lambda}_A^e}\bar{\lambda}_{\mathrm{A}}^e - \frac{1}{3}\sum_{\mathrm{B}}\frac{\partial\psi}{\partial\bar{\lambda}_{\mathrm{B}}^e}\bar{\lambda}_{\mathrm{B}}^e$$

as shown in the Appendix, from Eqs. (50) and (51) we deduce that:

$$p = K\log[J^e] \tag{53}$$

$$t_{\mathrm{A}} = 2G\log\left[\bar{\lambda}_{\mathrm{A}}^e\right]$$

Hence:

$$\tau_{\mathrm{A}} = K\log[J^e] + 2G\log\left[\bar{\lambda}_{\mathrm{A}}^e\right] \tag{54}$$

4.2. Yield functions

We consider three different yielding criteria defined through the following functions:

$$\begin{cases} \text{von Mises} & f = [2J_2]^{\frac{1}{2}} \\ \text{Drucker}-\text{Prager} & f = [2J_2]^{\frac{1}{2}} + \dfrac{\alpha}{3}I_1 \\ \text{Prager}-\text{Lode} & f = [2J_2]^{\frac{1}{2}} + \beta\left[\dfrac{27}{2}\right]^{\frac{1}{2}}J_3J_2^{-1} \end{cases} \tag{55}$$

with α and β material constants relative to the specific models. To particularize the discussion of the previous section to these yield criteria, we have only to compute their derivatives with respect to the stress invariants. In particular, reporting only the non-zero derivatives, we have:

$$\begin{cases} \text{von Mises} & \begin{cases} f_2 = [2J_2]^{-\frac{1}{2}} \\ f_{22} = -[2J_2]^{-\frac{3}{2}} \end{cases} \\ \text{Drucker}-\text{Prager} & \begin{cases} f_1 = \dfrac{\alpha}{3} \\ f_2 = [2J_2]^{-\frac{1}{2}} \\ f_{22} = -[2J_2]^{-\frac{3}{2}} \end{cases} \\ \text{Prager}-\text{Lode} & \begin{cases} f_2 = [2J_2]^{-\frac{1}{2}} - \beta\left[\dfrac{27}{2}\right]^{\frac{1}{2}} J_3 J_2^{-2} \\ f_3 = \beta\left[\dfrac{27}{2}\right]^{\frac{1}{2}} J_2^{-1} \\ f_{22} = [2J_2]^{-\frac{3}{2}} + 2\beta\left[\dfrac{27}{2}\right]^{\frac{1}{2}} J_3 J_2^{-3} \\ f_{23} = -\beta\left[\dfrac{27}{2}\right]^{\frac{1}{2}} J_2^{-2} \end{cases} \end{cases} \tag{56}$$

Finally, to make possible an easy comparison between the different yield criteria, we found it more convenient to express the material constants of each criterion in terms of a common material parameter set. In particular, indicating with σ_t and σ_c the magnitude of the initial yielding values in tension and compression, we get the following relations:

$$\begin{cases} \text{von Mises} & \begin{cases} \sigma_y = \left[\dfrac{2}{3}\right]^{\frac{1}{2}} \sigma_t \end{cases} \\ \text{Drucker}-\text{Prager} & \begin{cases} \sigma_y = 2\left[\dfrac{2}{3}\right]^{\frac{1}{2}} \dfrac{\sigma_c \sigma_t}{\sigma_c + \sigma_t} \\ \alpha = 3\left[\dfrac{2}{3}\right]^{\frac{1}{2}} \dfrac{\sigma_c - \sigma_t}{\sigma_c + \sigma_t} \end{cases} \\ \text{Prager}-\text{Lode} & \begin{cases} \sigma_y = 2\left[\dfrac{2}{3}\right]^{\frac{1}{2}} \dfrac{\sigma_c \sigma_t}{\sigma_c + \sigma_t} \\ \beta = \dfrac{\sigma_c - \sigma_t}{\sigma_c + \sigma_t} \end{cases} \end{cases} \tag{57}$$

5. Numerical examples

To show the performances of the plasticity framework discussed above, we now report the results of some numerical simulations. They are all obtained running a three-dimensional tri-linear isoparametric displacement-based finite element, implemented

into the finite element analysis program (Zienkiewicz and Taylor, 1989, 1991). The numerical simulations are organized as follows:

1. Uniaxial tension test
2. Perforated strip test
3. Cantilever beam test

The choice of the examples is consistent with the need to investigate the model response for simple stress states initially (in particular, one-dimensional states, such as in a uniaxial case) and then for more complicated stress states (in particular, multi-dimensional as well as non-proportional states, such as in a perforated strip and in a cantilever beam).

The elastic material properties are set equal to: $E = 10^4$ MPa, $\nu = 0.3$. For the plastic material properties we distinguish between two cases:

Material 1: with equal yielding thresholds in tension and compression.
In particular, we set: $\sigma_t = \sigma_c = 100$ MPa.
Material 2: with different yielding thresholds in tension and compression.
In particular, we set: $\sigma_t = 100$ MPa and $\sigma_c = 9/8\sigma_t$.

To investigate the model behaviors as well to check our implementation, all the tests have been performed first for the case of Material 1, a case in which they all return exactly the same answer. Then, all the tests have been performed for the case of Material 2, a case for which only the Drucker–Prager and the Prager–Lode models can be used. To condense the presentation of results, in the following we report in a single figure the response for Material 1 (only for the von Mises model) and the response for Material 2 (both for the Drucker–Prager and the Prager–Lode models).

5.1. Uniaxial tension test

The test is simulated on a cubic specimen, for which the boundary conditions are set such to produce a uniaxial state of stress. The specimen is modeled using a single element and is loaded controlling the displacements. A cyclic loading history (i.e. loading–unloading–reloading) is considered.

Fig. 1 shows the results for Material 1 (Mises model) and for Material 2 (Drucker–Prager and the Prager–Lode models) in terms of engineering stress versus engineering strain. As expected, for Material 2 the model response in tension and compression differs.

Table 2 reports some information relative to the convergence process for both sets of analyses. In particular, the table contains the following quantities:

- number of steps adopted to describe the loading history (*Steps*)
- total number of iterations during the whole solution process (*Iter.*)
- average number of iterations per step (*Steps/iter.*).

It is interesting to observe that: (1) the models show the same performance; (2) the average number of iterations per step is equal to 3, indicating a very fast convergence (in particular, super-quadratic).

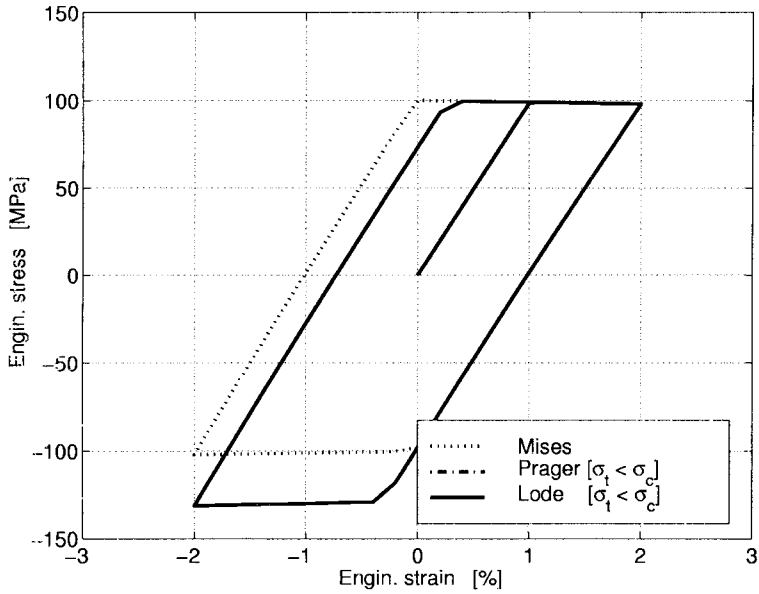

Fig. 1. Uniaxial tension test. Engineering stress versus engineering strain for Material 1 (von Mises model) and Material 2 (Drucker-Prager and Prager-Lode Models).

Table 2
Uniaxial tension test: convergence[a]

Material	Model type	Steps	Iter.	Steps/Iter.
1	von Mises	52	159	3
	Drucker–Prager	52	159	3
	Prager–Lode	52	159	3
2	Drucker–Prager	52	159	3
	Prager–Lode	52	159	3

[a] Number of steps per loading history, total number of iterations, average number of iterations per step for Material 1 and for Material 2.

5.2. Perforated strip test

To investigate more complex stress patterns, we consider a three-dimensional version of the perforated strip studied in Zienkiewicz and Taylor (1991, p. 245). The strip has dimension 36×20 mm with a central circular hole of diameter 10 mm and thickness equal to 1 mm. We consider a cyclic loading history (i.e. loading–unloading–reloading), applied controlling the displacements of the strip top boundary.

Due to symmetry conditions, only a quarter of the strip is discretized, in particular, Fig. 2 shows the finite-element mesh adopted. The relations between the reaction and the imposed displacement are plotted in Fig. 3.

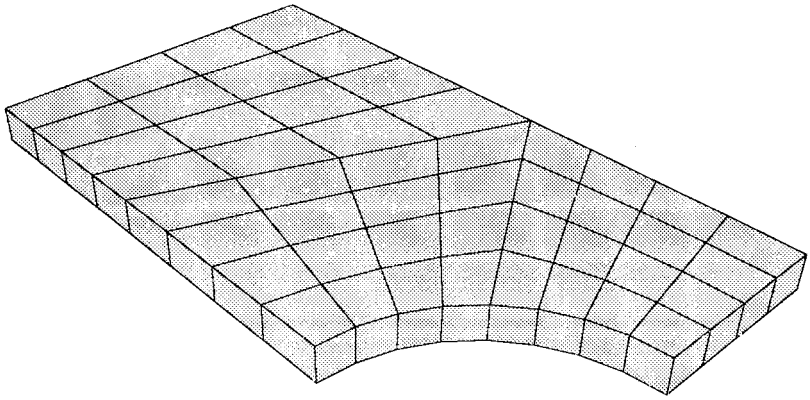

Fig. 2. Perforated strip test: finite-element mesh. Perspective view of the adopted finite-element mesh.

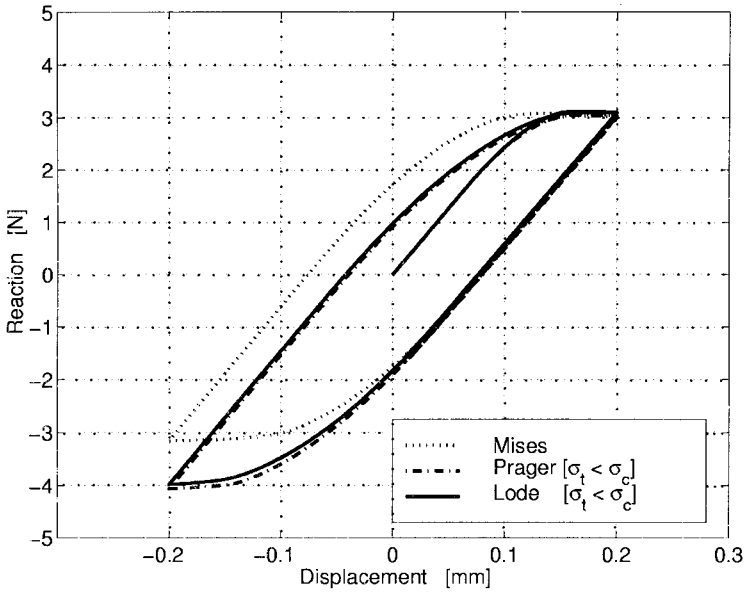

Fig. 3. Perforated strip test. Total reaction versus improved displacement for Material 1 (von Mises model) and Material 2 (Drucker-Prager and Prager-Lode models).

As for the uniaxial tension test, Table 3 reports some information relative to the convergence process for both sets of analyses. Again, it is possible to observe that: (1) the three models show very close performance; (2) the average number of iterations per step is equal to 4, which is consistent with a quadratic asymptotic rate of convergence.

5.3. Cantilever beam test

Finally, we consider a cantilever beam. The beam has dimensions: length $L = 20$ mm, height $h = 6$ mm, thickness $t = 1$ mm; it is clamped at one end and loaded at the

Table 3
Perforated strip test: convergence[a]

Material	Model type	Steps	Iter	Steps/Iter.
1	von Mises	120	496	4
	Drucker–Prager	120	496	4
	Prager–Lode	120	496	4
2	Drucker–Prager	120	478	4
	Prager–Lode	120	482	4

[a] Number of steps per loading history, total number of iterations, average number of iterations per step for Material 1 and for Material 2.

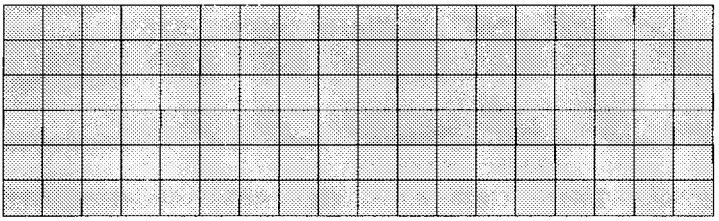

Fig. 4. Cantilever beam test: perspective view of the adopted finite-element mesh.

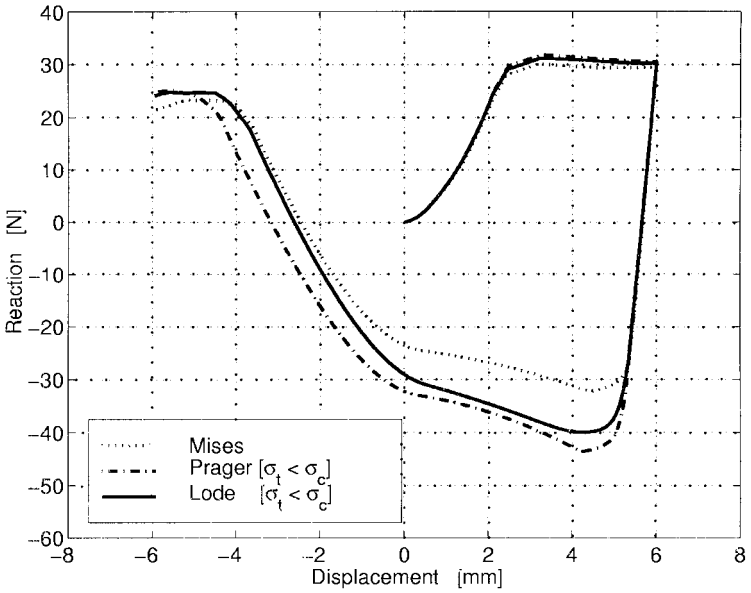

Fig. 5. Cantilever beam test. Total reaction versus improved displacement for Material 1 (von Mises model) and Material 2 (Drucker-Prager and Prager-Lode models).

Table 4
Cantilever beam test: convergence[a]

Material	Model type	Steps	Iter	Steps/Iter.
1	von Mises	300	1205	4
	Drucker–Prager	300	1205	4
	Prager–Lode	300	1205	4
2	Drucker–Prager	300	1216	4
	Prager–Lode	300	1214	4

[a] Number of steps per loading history, total number of iterations, average number of iterations per step for Material 1 and for Material 2.

other end controlling the vertical displacements. In particular. we consider a cyclic loading history (i.e. loading–unloading–reloading).

Fig. 4 shows the finite-element mesh adopted. The relations between the total reaction and the imposed displacement are plotted in Fig. 5.

As for the previous tests, Table 4 reports some information relative to the convergence process for both sets of analyses. Again, it is possible to observe that: (1) the three models show relatively close performance; (2) the average number of iterations per step is equal to 4, which is again consistent with a quadratic rate of convergence.

6. Conclusions

In the present paper we devise and discuss a flexible solution algorithm for associative isotropic elasto-plastic materials, i.e. for materials whose elastic and plastic behaviors are described respectively through an isotropic free-energy function, an isotropic yield function and an associative flow rule. The discussion is relative to a large deformation regime, while no hardening mechanisms are included in the modelling.

The algorithm is based on a combination of the operator split method and of a return map scheme. The main advantages of the proposed approach are: (1) the independence from the specific form of the free-energy and of the yield criterion; (2) the similarity between the adopted return map and the one commonly used in a small deformation regime, which clearly makes possible the easy inclusion of models from previously developed constitutive libraries.

To show the algorithm flexibility, the discussion is specialized to the case of three yield criteria (i.e. von Mises, Drucker–Prager and Prager–Lode). Finally, some test problems are numerically studied to show its performance.

Appendix A. Some algebra

Remark A1. *From Eq. (7), we get:*

$$\tau_A = 2\frac{\partial \psi}{\partial\left[(\lambda_A^e)^2\right]}(\lambda_A^e)^2 = 2\sum_{B=1}^{3}\frac{\partial \psi}{\partial \lambda_B^e}\frac{\partial \lambda_B^e}{\left[(\lambda_A^e)^2\right]}(\lambda_A^e)^2 \tag{A1}$$

Noting that:

$$\frac{\partial\left[(\lambda_A^e)^2\right]}{\partial \lambda_B^e} = 2\lambda_A^e \delta_{AB} \tag{A2}$$

and hence that:

$$\frac{\partial \lambda_B^e}{\partial\left[(\lambda_A^e)^2\right]} = \frac{1}{2\lambda_A^e}\delta_{AB} \tag{A3}$$

Eq. (A1) reduces to:

$$\tau_A = \sum_{B=1}^{3}\frac{\partial \psi}{\partial \lambda_B^e}\lambda_A^e \delta_{AB} = \frac{\partial \psi}{\partial \lambda_A^e}\lambda_A^e \tag{A4}$$

Remark A2. *Assume a free energy ψ of the type:*

$$\psi = \psi(J^e, \bar{\lambda}_A^e) \tag{A5}$$

where J^e and $\bar{\lambda}_A^e$ are the elastic jacobian and the elastic deviatoric principal stretches, respectively defined as:

$$J^e = \lambda_1^e \lambda_2^e \lambda_3^e,\ \bar{\lambda}_A^e = (J^e)^{-\frac{1}{3}}\lambda_A^e \tag{A6}$$

Accordingly, we have:

$$\frac{\partial \psi}{\partial \lambda_A^e} = \frac{\partial \psi}{\partial J^e}\frac{\partial J^e}{\partial \lambda_A^e} + \sum_{B=1}^{3}\frac{\partial \psi}{\partial \bar{\lambda}_B^e}\frac{\partial \bar{\lambda}_B^e}{\partial \lambda_A^e} \tag{A7}$$

Since:

$$\frac{\partial J^e}{\partial \lambda_A^e} = \frac{J^e}{\lambda_A^e} \tag{A8}$$

$$\frac{\partial \bar{\lambda}_B^e}{\partial \lambda_A^e} = -\frac{1}{3}(J^e)^{-\frac{1}{3}}\frac{\lambda_B^e}{\lambda_A^e} + (J^e)^{-\frac{1}{3}}\delta_{AB}$$

we find:

$$\tau_A = \frac{\partial \psi}{\partial J^e} J^e + \frac{\partial \psi}{\partial \bar{\lambda}^e_A} \bar{\lambda}^e_A - \frac{1}{3} \sum_{B=1}^{3} \frac{\partial \psi}{\partial \bar{\lambda}^e_B} \bar{\lambda}^e_B \tag{A9}$$

Recalling that:

$$\sum_{A=1}^{3} \tau_A = 3p \tag{A10}$$

$$t_A = \tau_A - p$$

we conclude that:

$$p = \frac{\partial \psi}{\partial J^e} J^e \tag{A11}$$

$$t_A = \frac{\partial \psi}{\partial \bar{\lambda}^e_A} \bar{\lambda}^e_A - \frac{1}{3} \sum_{B=1}^{3} \frac{\partial \psi}{\partial \bar{\lambda}^e_B} \bar{\lambda}^e_B$$

References

Armero, F., Simo, J.C., 1993. A priori stability estimates and unconditionally stable product formula algorithms for nonlinear coupled thermoplasticity. International Journal of Plasticity 9, 749–782.

Auricchio, F., Taylor, R.L., 1995. Two material models for cyclic plasticity: non-linear kinematic hardening and generalized plasticity. International Journal of Plasticity 11, 65–98.

Bathe, K.J., 1982. Finite Element Procedures in Engineering Analysis. Prentice Hall.

Gurtin, M.E., 1981. An Introduction to Continuum Mechanics. Academic Press.

Lee, E.H., 1969. Elastic-plastic deformation at finite strains. Journal of Applied Mechanics 36, 1–6.

Lubliner, J., 1990. Plasticity Theory. Macmillan.

Mandel, J., 1974. Thermodynamics and plasticity. In: Delgado Dominger, J.J., Nina, M.N.R., Whitelaw, J.H. (Eds.), Foundations of Continuum Thermodynamics. pp. 283–304.

Protter, M.H., Charles, B., Morrey, Jr., B., 1992. A First Course in Real Analysis. Springer–Verlag.

Simo, J.C., 1992. Algorithms for static and dynamic multiplicative plasticity that preserve the classical return mapping schemes of the infinitesimal theory. Computer Methods in Applied Mechanics and Engineering 99, 61–112.

Simo, J.C., 1999. Topics on the numerical analysis and simulation of plasticity. In: Ciarlet, P.G., Lions, J.L. (Eds.), Handbook of Numerical Analysis, Vol. III. Elsevier Science Publisher B.V.

Simo, J.C., Hughes, T.J.R., 1998. Computational Inelasticity. Springer-Verlag.

Simo, J.C., Meschke, G., 1993. A new class of algorithms for classical plasticity extended to finite strains, applications to geomaterials. Computational Mechanics 11, 253–278.

Simo, J.C., Taylor, R.L., 1985. Consistent tangent operators for rate-independent elasto-plasticity. Computer Methods in Applied Mechanics and Engineering 48, 101.

Zienkiewicz, O.C., Taylor, R.L., 1989. The Finite Element Method, Vol. I, 4th Edition. McGraw Hill, New York.

Zienkiewicz, O.C., Taylor, R.L., 1991. The Finite Element Method, Vol. II, 4th Edition. McGraw Hill, New York.